Lithos 113 (2009) 583–594

Contents lists available at ScienceDirect

Lithos

journal homepage: www.elsevier.com/locate/lithos

OIB-like, heterogeneous mantle sources of Permian basaltic magmatism in the western Tarim Basin, NW China: Implications for a possible Permian large igneous province

Mei-Fu Zhou [a,b,*], Jun-Hong Zhao [a,b], Chang-Yi Jiang [c], Jian-Feng Gao [a], Wei Wang [d], Sheng-Hong Yang [a]

[a] Department of Earth Sciences, University of Hong Kong, Hong Kong, China
[b] State Key Laboratory of Ore Deposit Geochemistry, Institute of Geochemistry, Chinese Academy of Sciences, Guiyang, China
[c] School of Earth Resources, Chang'an University, Xian, China
[d] Institute of Geology and Geophysics, Chinese Academy of Sciences, Beijing, China

ARTICLE INFO

Article history:
Received 4 December 2008
Accepted 12 June 2009
Available online 2 July 2009

Keywords:
Permian basalt
Geochemistry
Heterogeneous mantle source
Tarim Basin
Large igneous province

ABSTRACT

Permian basalts are widely distributed in the Tarim Basin and surrounding areas of NW China. The magmatism is represented by basaltic flows in Keping and mafic and ultramafic dykes in Silurian–Devonian strata in Bachu, southwestern Tarim Basin. The basalts in Keping have SiO_2 (44.1%–55.5 wt.%) and total alkalis ($Na_2O+K_2O=3.20$–7.79 wt.%) similar to the mafic dykes in Bachu, but with much higher TiO_2 (3.53–4.33 wt.%). An ultramafic dyke has relatively low SiO_2 (44.6–43.2 wt.%) and high MgO (19.0–20.2 wt.%), reflecting the abundance of cumulate olivine. All the rocks, including both lavas and dykes, have parallel, mantle-normalized trace element patterns enriched in Rb, Ba, Th, Nb, Ta, Zr, Hf, and light rare earth elements (LREE). The basalts have higher initial $^{87}Sr/^{86}Sr$ ratios (0.7064 to 0.7080) and lower $\varepsilon Nd(t)$ values (−2.66 to −9.27) than the dykes (initial $^{87}Sr/^{86}Sr$ ratios range from 0.7048 to 0.7052 and $\varepsilon Nd(t)$ values from +1.64 to +5.16). Both the basalts and dykes show a narrow range of $^{206}Pb/^{204}Pb$ (17.87–18.77), $^{207}Pb/^{204}Pb$ (15.52–15.58) and $^{208}Pb/^{204}Pb$ (38.38–39.04) ratios. The dykes do not show significant crustal contamination and were derived from an OIB-like, asthenospheric mantle source. In contrast, the basaltic flows show variable degrees (up to 10%) of crustal contamination and were derived from an OIB-like, but isotopically more enriched, asthenospheric mantle source. Olivine from the ultramafic dyke has Fo values up to 85, corresponding to a melt temperature of 1300 °C and a melt Mg# of 63. The Tarim Basin magmatism reflects partial melting of heterogeneous mantle sources related to a major mantle plume. Spatially and temporally associated mafic–ultramafic and syenitic intrusions and volcanic rocks form the ~275 Ma Tarim large igneous province.

1. Introduction

Large igneous provinces (LIPs), composed of basalt and mafic–ultramafic intrusions, are the products of voluminous basaltic magmatism and important for understanding the thermal evolution of Earth (Mahoney and Coffin, 1997; Pirajno, 2000; Ernst and Buchan, 2001, 2003). Permian mafic–ultramafic intrusions and flood basalts are widespread in the Eurasian continent and include the well-known ~251-Ma Siberian Traps in Russia (Campbell et al., 1992; Lightfoot et al., 1993; Arndt et al., 1998; Reichow et al., 2009), and the ~260-Ma Emeishan LIP (ELIP) in SW China (Chung and Jahn, 1995; Xu et al., 2001; Zhou et al., 2002). Volcanic rocks and intrusions are also abundant in the Tarim Basin and surrounding regions of NW China and they may represent another Permian LIP (Yang et al., 1996; Chen et al., 1997, 1999; Jiang et al., 2004a,b; Yang et al., 2005, 2006a,b; Jiang et al., 2006b; Yang et al., 2007; Zhang et al., 2008; Pirajno et al., 2009). Identifying the processes that produced the widespread Permian magmatism across the entire Eurasian continent is crucial for understanding the tectonic evolution of the region.

Despite numerous studies, the origin of the Permian basalts and mafic–ultramafic intrusions in the Tarim Basin are poorly understood, and the nature of their mantle sources is still unknown. Likewise, the processes that produced such extensive magmatism are unclear. A detailed investigation of the geochemical characters of these rocks should provide information on their origin and possible mantle sources in order to determine whether or not they were produced by a mantle plume and form part of a Permian LIP.

This paper focuses on the Permian basalts in the Keping area and mafic and ultramafic dykes at Bachu in the western Tarim Basin (Fig. 1) and presents new major and trace element and Sr–Nd–Pb isotope data for these rocks. This new dataset is utilized to investigate the possible nature

* Corresponding author. Department of Earth Sciences, University of Hong Kong, Hong Kong, China.
E-mail address: mfzhou@hkucc.hku.hk (M.-F. Zhou).

0024-4937/$ – see front matter
doi:10.1016/j.lithos.2009.06.027

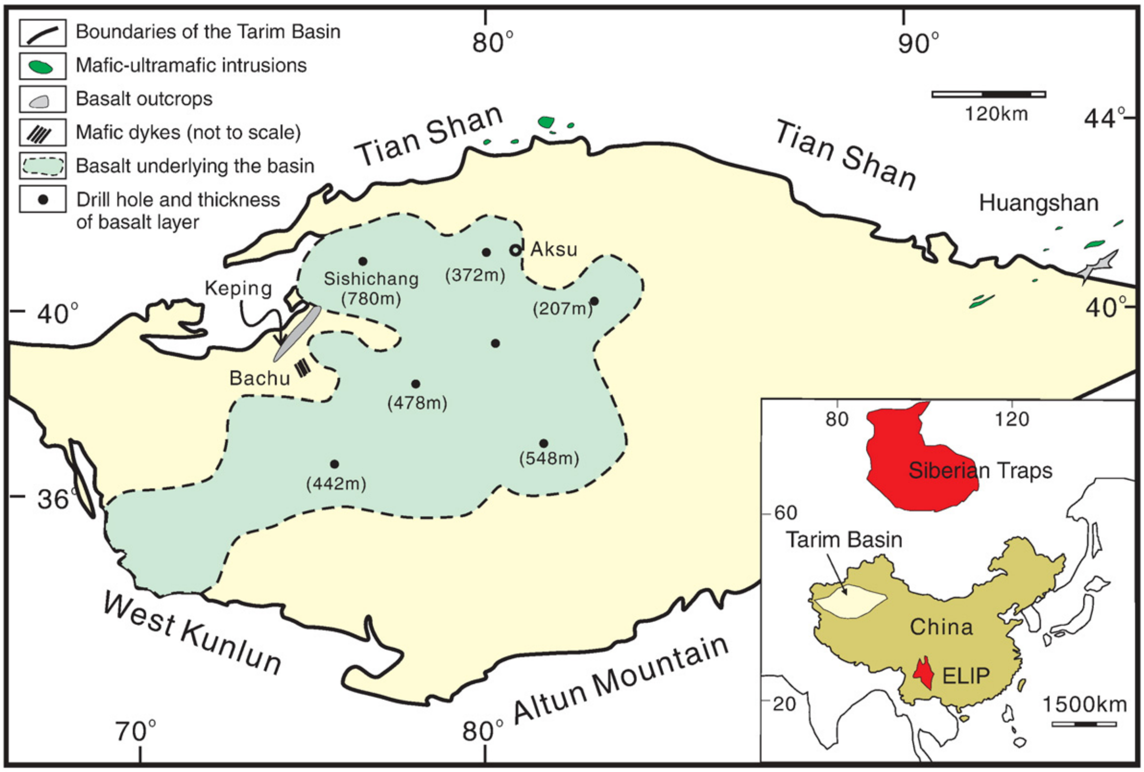

Fig. 1. A simplified geological map showing the distribution of Permian basalts underlying the Tarim Basin and outcrops in the Keping region, western Tarim. A Permian dyke swarm in Bachu is also shown. Note that the basalts shown represent the minimum distribution based on available oil company drill holes in the basin (Yang et al., 2007). The lower right inset shows the locations of the Siberia Traps to the north and the ELIP to the south.

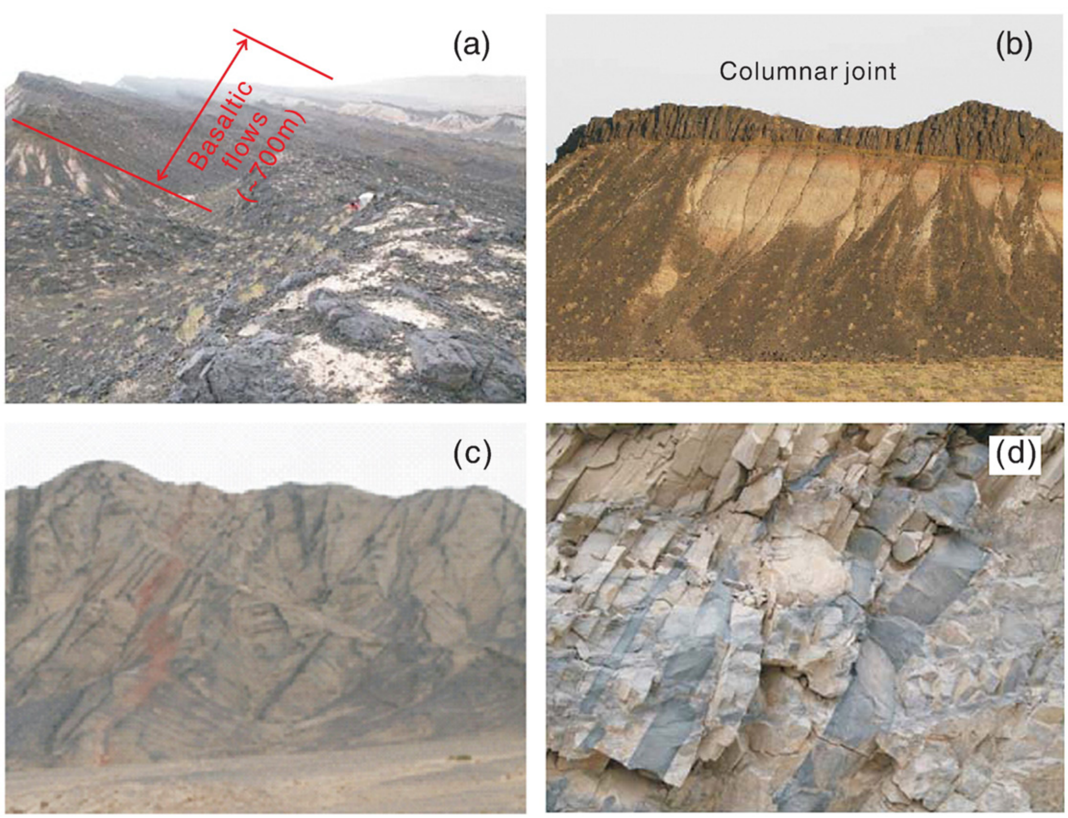

Fig. 2. Field photos showing the flood basalts in the Permian strata near Keping (a and b). The flood basalts are interlayered with Permian sandstones and include several flows. The basalts are well exposed along the margin of the Tarim Basin and are visible for at least 40 km along strike. Near Keping, mafic dyke swarms (dark in color) in the Devonian strata (c and d) are abundant and remarkably well preserved.

of the parental magmas and mantle sources in order to determine whether or not they originated from a mantle plume. Based on the regional distribution, probable age and geochemistry of these rocks, we suggest that they represent part of a LIP, which we refer to as the Tarim LIP.

2. Geological background

2.1. Regional geology

The Tarim Basin of NW China is bounded by the Tianshan Mountains to the north and west and the West Kunlun and Altun Mountains to the south (Fig. 1). The Tianshan Mountains are part of the Central Asian Orogenic Belt composed of Paleozoic ophiolites, arc volcanic rocks and continental fragments (Jahn et al., 2000a,b). Both the Kunlun and Altun Mountains are part of the northern Tibetan Plateau. The Tarim Basin has a mainly Precambrian basement probably composed of Archean and Neoproterozoic crystalline rocks (Xinjiang Bureau of Geology and Mineral Resources (XJBGMR), 1993). The crystalline basement is overlain by a thick sedimentary sequence that includes Ordovician, Permian and Cretaceous strata (Xinjiang Bureau of Geology and Mineral Resources (XJBGMR), 1993; Jia, 1997; Zhang, 2003; Jia et al., 2004). The Permian strata in the Tarim Basin consist mainly of a volcanic-sedimentary sequence composed of clastic rocks, muddy limestones and mafic volcanic rocks.

2.2. Permian igneous rocks in the Tarim Basin

Widespread Permian basalts have recently been discovered in the Tarim Basin and adjacent areas (Jiang et al., 2004a,b,c; Yang et al., 2005; Jiang et al., 2006a,b; Yang et al., 2006a,b, 2007; Zhang et al., 2008). Sparse outcrops around the basin and drill holes within the basin reveal a well-developed Permian section composed chiefly of volcanic rocks and carbonates. These rocks occur mainly in the western and southwestern parts of the basin (Fig. 1). The strata are divided into the lower to middle Permian Kupukuziman Formation and the overlying middle Permian Kaipaizileike Formation (XBRMG, 1993). The spatial distribution of the Permian basalts and sedimentary strata in the Keping area are readily apparent in Fig. 2a and b. Drill holes at Hade and Sishichang (Fig. 1) penetrated 207 m and 780 m of basalt, respectively. Because much of the volcanic sequence occurs in the subsurface, and exposures around the basin margin are difficult to access, its full extent is not clear. However, geophysical and borehole data, suggest that the Permian basalts (including related tuff and tuffaceous sedimentary rocks) may extend over an area of ca. 250,000 km^2 in the Tarim Basin (Jia, 1997; Chen et al., 2006). Drill-hole data indicate that the volcanic rocks range from ~200 to ~800 m thick with an estimated average thickness of ~ 300 m, suggesting a volume of more than 75,000 km^3 (Fig. 1) (Jia et al., 2004; Jiang et al., 2004b; Chen et al., 2006).

Six basaltic flows of the Kaipaizileike Formation are interlayered with Permian fluvial sedimentary rocks at the edge of the basin near Keping. The sequence, which has a total thickness of ca. 530 m, consists mainly of basaltic flows with small amounts of intercalated Permian mudstone, siltstone and muddy limestone. Individual basalt flows range from several tens of meters to more than 300 m thick. One flow has well-developed columnar jointing (Fig. 2b).

Permian intrusions in the Tarim Basin and surrounding areas include felsic and mafic–ultramafic plutons and numerous dykes (e.g., Jiang et al., 2004a,b,c; Yang et al., 2005, 2006a,b; Zhang et al., 2008). North–northwest-trending diabase dyke swarms in the Bachu area intrude Silurian, Devonian, Carboniferous and Early Permian strata (Fig. 2).

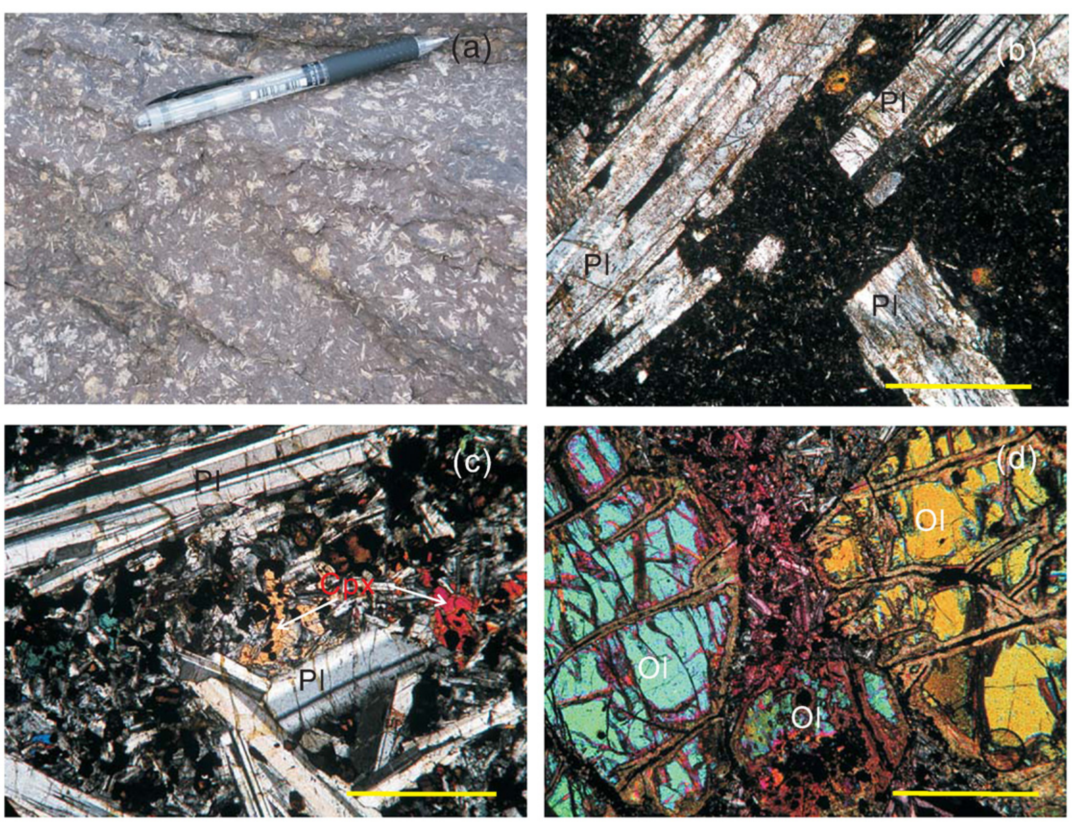

Fig. 3. (a) Porphyritic texture of basalts for Keping, showing abundant plagioclase phenocrysts; (b) euhedral plagioclase set in the fine-grained matrix consisting of plagioclase and clinopyroxene; (c) porphyritic texture of diabase dyke in Bachu, composed of plagioclase and clinopyroxene phenocrysts; and (d) olivine-rich rocks from the ultramafic dyke in Bachu. Pl—plagioclase; Cpx—clinopyroxene; Ol—olivine. The scale bar is 1 mm.

Table 1
Major and trace elements for the basalts and mafic dykes from the Tarim Basin, NW China.

	Mafic dykes														Ultramafic dykes			
	XHZ34	XHZ36	XHZ37	XHZ40	XHZ44	XHZ45	XHZ47	XHZ49	XHZ51	XHZ53	XHZ54	XHZ55	XHZ57	XHZ60	XHZ62	XHZ63	XHZ64	XHZ65
Major element (wt.%)																		
SiO_2	47.67	47.68	49.93	49.91	50.66	54.11	46.79	45.66	47.33	46.78	46.76	46.71	45.98	49.24	42.99	42.89	43.02	43.21
TiO_2	3.41	3.20	2.44	2.46	2.49	1.73	3.12	2.60	3.27	3.24	3.32	3.29	3.26	2.93	1.59	1.63	1.57	1.60
Al_2O_3	14.48	15.07	16.17	16.45	16.40	16.55	14.34	13.22	14.21	14.84	14.27	14.22	14.12	15.06	6.63	6.56	6.30	6.64
Fe_2O_3	13.56	13.42	10.40	10.59	10.67	8.92	14.23	13.23	13.91	13.77	14.22	14.15	14.40	12.33	14.57	14.67	14.97	14.32
MnO	0.19	0.38	0.17	0.17	0.17	0.14	0.18	0.18	0.20	0.20	0.20	0.20	0.18	0.19	0.16	0.15	0.15	0.16
MgO	4.74	4.54	3.79	3.81	3.75	2.82	5.67	7.94	4.80	4.82	5.08	4.95	5.38	4.25	18.73	18.77	19.55	18.17
CaO	7.86	8.08	6.61	7.13	6.67	5.02	6.91	9.55	6.84	7.47	7.39	7.81	7.95	6.86	9.93	10.04	9.92	10.32
Na_2O	3.48	3.33	4.63	4.78	4.71	5.50	4.22	3.38	4.36	4.96	4.46	4.42	4.48	4.77	0.82	0.74	0.71	0.71
K_2O	1.78	1.39	2.03	1.49	1.84	2.10	0.20	0.31	1.71	0.12	1.02	1.01	0.63	0.85	0.17	0.16	0.17	0.16
P_2O_5	0.72	0.66	0.52	0.50	0.52	0.62	0.56	0.45	0.61	0.64	0.60	0.59	0.50	0.56	0.16	0.16	0.15	0.16
LOI	1.80	2.10	3.20	2.67	2.03	2.43	3.63	3.11	2.43	2.94	2.69	2.62	3.09	2.89	4.13	4.07	3.44	4.17
Total	99.70	99.85	99.89	99.99	99.91	99.93	99.85	99.62	99.67	99.76	100.01	99.97	99.97	99.94	99.87	99.84	99.94	99.61
Trace element (ppm)																		
Sc	22.9	21.2	21.2	21.6	20.2	14.8	24.9	28.2	23.3	23.9	21.0	21.5	22.4	22.0	29.8	35.0	29.5	31.8
V	234	214	185	198	182	95	235	205	208	250	262	206	232	217	216	227	211	222
Cr	3.0	15.2	10.3	15.5	10.5	5.9	34.7	212	1.0	4.3	3.9	7.0	2.1	4.1	1078.0	1138.9	1067.4	1129.5
Co	30.4	21.4	30.0	31.6	27.3	19.0	47.2	49.1	38.0	36.2	36.6	36.7	40.4	31.8	102.7	103.7	107.8	98.1
Ni	9.6	8.1	10.2	14.5	10.7	5.3	54.0	126	11.1	8.42	13.2	11.9	33.8	8.3	563	578	602	560
Cu	41.4	33.7	31.8	34.6	26.5	45.5	95.6	126	47.8	41.8	51.9	51.1	112.1	24.6	95.9	98.6	99.6	90.9
Zn	229	253	131	133	115	108	145	127	134	146	126	150	141	144	110	108	109	106
Ga	27.2	27.5	26.0	25.9	24.8	26.0	24.4	20.8	22.5	24.7	21.3	21.6	23.1	24.0	11.7	12.3	11.2	11.7
Ge	1.53	1.66	1.45	1.36	1.40	1.30	1.81	1.68	1.49	1.63	1.46	1.35	1.45	2.01	1.45	1.46	1.46	1.51
Rb	60.6	49.7	33.7	24.5	39.9	44.0	6.0	10.1	26.7	1.8	15.0	15.4	12.8	14.4	8.5	9.4	9.7	8.0
Sr	659	724	606	609	588	432	557	654	517	564	434	482	403	533	180	208	180	182
Y	38.7	38.9	34.3	33.2	36.3	43.4	36.7	30.4	36.2	38.2	30.7	33.0	30.4	34.9	14.6	15.4	13.3	14.7
Zr	342	362	325	317	318	417	297	242	327	338	320	311	286	338	110	107	96	111
Nb	69	62	44	43	46	58	42	33.9	44.4	45.6	44.0	42.2	40.5	49.3	14.6	14.2	13.1	14.9
Cs	1.61	3.06	0.63	0.42	0.33	0.25	2.42	1.39	0.41	0.66	0.25	0.40	0.26	1.58	2.29	3.94	2.33	2.69
Ba	453	406	730	790	824	1158	145	107	927	107	488	557	566	518	68	71	73	65
La	49	49	49	46	49	63	39	32.1	41.9	46.5	37.3	38.5	37.4	48.9	12.2	12.7	11.7	12.5
Ce	107	109	105	100	108	127	88	72.5	101	104	94	93	87	109	29	29	27	29
Pr	13.3	13.6	12.4	11.8	12.4	14.7	10.3	8.47	11.1	11.7	9.60	10.1	9.51	11.7	3.61	3.79	3.41	3.69
Nd	56.9	58.4	51.5	49.4	50.7	59.6	43.8	36.6	46.7	48.8	40.6	42.2	40.2	47.1	15.7	16.3	15.0	16.1
Sm	12.8	12.7	10.8	10.44	10.40	11.78	9.90	8.39	10.38	10.68	8.86	9.40	8.79	10.35	3.90	4.00	3.69	3.86
Eu	3.98	3.52	3.40	3.21	3.22	3.59	3.14	2.66	3.27	3.39	2.82	3.01	2.76	3.07	1.23	1.24	1.17	1.23
Gd	10.7	10.5	9.09	8.72	8.48	9.84	8.40	6.92	8.62	8.77	7.48	7.89	7.42	8.38	3.35	3.44	3.18	3.39
Tb	1.69	1.66	1.40	1.36	1.36	1.55	1.32	1.09	1.39	1.40	1.17	1.22	1.17	1.28	0.54	0.55	0.52	0.55
Dy	9.21	9.26	7.96	7.50	7.17	8.45	7.14	6.05	7.16	7.40	6.16	6.66	6.18	6.86	2.88	3.08	2.82	3.00
Ho	1.67	1.64	1.46	1.37	1.35	1.59	1.31	1.09	1.34	1.40	1.15	1.25	1.13	1.28	0.58	0.55	0.49	0.56
Er	4.13	4.16	3.85	3.56	3.57	4.17	3.43	2.94	3.44	3.76	2.99	3.21	2.92	3.34	1.39	1.45	1.35	1.41
Tm	0.53	0.53	0.49	0.48	0.46	0.55	0.44	0.37	0.43	0.47	0.38	0.43	0.35	0.43	0.17	0.18	0.15	0.18
Yb	3.07	3.03	2.87	2.81	2.65	3.29	2.54	2.13	2.65	2.76	2.25	2.40	2.13	2.49	0.99	1.05	0.95	1.01
Lu	0.43	0.42	0.41	0.41	0.38	0.48	0.35	0.29	0.36	0.39	0.32	0.35	0.29	0.33	0.13	0.13	0.13	0.14
Hf	10.15	9.72	9.06	8.24	8.20	10.41	6.84	5.47	7.46	7.85	7.14	7.05	6.57	7.54	2.77	2.59	2.52	2.81
Ta	4.90	4.42	3.17	2.93	2.84	3.54	2.52	2.08	2.69	2.81	2.62	2.49	2.40	2.96	0.94	0.89	0.84	0.95
Pb	42.53	50.22	5.90	4.77	4.58	5.51	25.83	2.41	3.50	11.35	3.05	2.43	3.82	7.56	1.29	1.22	1.22	1.24
Th	4.09	3.69	7.24	5.97	6.28	8.21	3.73	3.33	3.74	4.14	3.45	3.44	3.88	5.58	1.30	1.34	1.24	1.40
U	2.25	2.58	1.86	1.68	1.43	1.90	1.24	0.91	1.57	1.94	1.41	1.21	1.11	1.33	0.34	0.34	0.31	0.38

Some of the syenitic and mafic–ultramafic bodies in the region have been interpreted as parts of a large layered intrusion (Zhang et al., 2008), but this interpretation needs to be confirmed by seismics.

3. Petrography

The basalts are fine-grained, holocrystalline rocks with a few modal percent of plagioclase and clinopyroxene phenocrysts in an intersertal groundmass composed of plagioclase, clinopyroxene and oxides with minor olivine. One flow has abundant plagioclase phenocrysts (50 modal%) (Fig. 3a, b), whereas several are aphyric. Some of the basalts are vesicular and amygdaloidal.

The diabase dykes at Bachu have similar textures to the basalts but are slightly coarser grained (Fig. 3c). The ultramafic dykes are highly porphyritic with 40–60 modal% phenocrysts, chiefly olivine accompanied by minor clinopyroxene. The olivine phenocrysts are euhedral to subhedral and up to 2.5 mm in diameter (Fig. 3d).

4. Analytical methods

4.1. Electron microprobe analyses

Major element compositions of clinopyroxene and olivine were determined with a JEOL JXA-8100 electron microprobe at the Guangzhou Institute of Geochemistry, Chinese Academy of Sciences. The analyses were performed with a voltage of 15 keV and a sample beam of 10 nA focused to a spot of ~2 μm in diameter. Natural mineral standards were used for calibration and a PAP correction procedure was applied to the data (Pouchou and Pichoir, 1991). The precision of the analyses is better than 5% for major elements.

4.2. Major and trace element analyses

Major element oxides were analyzed by X-ray fluorescence at the University of Hong Kong using the analytical procedures of Zhou et al.

Basaltic flows																
AQI-02	AQI-05	AQ2-01	AQ2-06	AQ3-3	AQ3-8	AQ3-10	AQ4-2	AQ5-2	AQ6-2	AQ7-2	AQ7-4	AQ8-2	AQ8-8	AQY1-2	AQY2-2	AQY4-4
44.44	43.82	44.32	44.11	45.12	44.80	45.03	43.55	43.26	46.71	44.81	41.42	47.60	44.76	44.59	45.56	47.31
3.57	3.93	3.89	3.80	3.80	3.74	3.46	4.13	3.69	3.89	3.92	3.35	3.73	3.68	4.15	3.94	3.82
14.90	14.29	14.74	14.73	15.03	15.03	15.72	15.60	15.19	17.14	15.80	14.61	14.39	15.23	13.96	14.36	14.34
15.85	16.37	16.36	16.14	14.96	15.14	14.26	15.92	13.23	12.75	14.73	12.34	13.40	14.92	15.93	15.46	13.21
0.18	0.19	0.19	0.19	0.20	0.20	0.19	0.15	0.25	0.13	0.13	0.26	0.20	0.19	0.21	0.21	0.24
6.29	5.43	5.42	5.61	5.83	6.39	6.99	3.62	2.66	3.46	2.05	2.17	5.82	6.63	6.08	6.26	5.81
7.89	7.99	8.08	7.88	8.53	8.34	7.96	9.52	8.04	8.98	7.70	11.01	8.45	7.93	7.72	7.96	9.49
3.06	3.22	2.94	2.66	2.72	2.87	2.59	3.30	5.06	3.21	4.89	4.42	2.88	2.60	2.63	2.77	3.10
1.26	1.49	1.51	1.80	1.22	1.19	1.04	1.22	1.28	1.26	1.39	2.11	1.37	1.13	1.37	1.32	0.89
0.87	0.97	0.98	0.97	0.96	0.94	0.87	0.99	0.94	0.99	1.05	0.85	0.91	0.92	1.21	1.08	0.87
1.69	2.22	1.47	1.68	1.34	1.37	1.94	2.01	5.91	1.28	3.88	7.28	0.86	1.91	1.77	1.46	0.85
100.00	99.93	99.89	99.59	99.69	99.99	100.05	100.01	99.51	99.79	100.35	99.82	99.61	99.89	99.63	100.36	99.92
19.7	24.6	20.2	21.1	22.2	25.1	23.5	25.1	23.2	25.2	26.8	22.8	29.9	22.8	29.3	28.9	30.7
183	221	192	209	210	266	254	253	189	263	175	148	285	245	277	284	276
56.4	48.4	52.0	53.2	62.9	81.6	92.6	69.7	45.7	60.5	57.6	49.2	76.9	72.5	70.2	73.3	77.3
40.1	43.3	38.8	42.8	45.3	60.1	58.4	48.4	37.1	43.2	45.6	38.6	53.6	52.2	57.0	54.9	59.9
90.7	59.8	83.0	72.7	82.9	98.1	101	91.8	11.3	23.7	7.3	5.2	62.7	62.0	64.8	60.7	63.5
38.4	48.7	43.0	44.8	41.1	58.1	50.4	49.8	39.6	37.1	38.8	39.8	63.8	48.3	71.4	62.6	64.8
145	154	142	149	150	165	148	137	113	142	121	121	162	132	191	163	163
26.0	26.9	26.4	24.9	25.5	25.1	24.4	25.2	22.4	25.0	26.8	19.5	26.8	21.7	29.1	25.3	27.7
2.46	2.63	2.49	2.47	2.44	2.47	2.10	2.56	2.09	2.39	2.51	1.93	4.71	3.91	5.38	4.64	4.69
29.9	33.2	22.7	23.7	28.5	25.9	22.8	22.9	20.2	24.9	17.4	32.1	26.6	18.1	29.5	26.9	11.2
522	443	493	848	480	529	428	462	1112	447	1190	702	326	322	334	378	422
45.3	50.3	48.5	47.1	49.6	43.3	43.6	44.3	40.7	41.4	49.9	42.1	43.7	40.8	44.9	45.6	44.2
291	321	285	266	296	284	307	270	280	277	299	259	296	276	357	337	280
28.6	36.5	31.4	29.3	29.3	30.2	27.0	29.0	27.4	30.5	31.7	25.5	31.0	30.7	38.7	39.0	28.5
1.33	1.50	0.11	0.21	0.51	0.93	0.43	0.07	1.48	0.30	0.17	3.84	0.29	0.46	0.22	0.42	0.61
772	897	681	887	647	599	570	607	780	634	583	1187	709	625	739	702	995
36.1	41.2	38.6	37.9	37.8	35.2	35.9	35.1	35.1	35.7	42.1	34.5	47.4	40.5	49.7	46.8	45.4
70	82	75	71	69	67	65	65	64	70	80	60	99	81	101	100	89
10.3	12.5	11.2	10.9	10.1	9.84	9.58	9.98	10.0	10.2	11.6	9.4	11.6	10.5	12.6	12.2	11.0
42.6	54.8	48.8	48.7	43.1	45.7	40.2	44.6	44.7	44.2	50.1	41.7	47.9	43.4	54.4	49.4	47.0
9.33	10.8	10.3	10.4	9.43	9.08	9.00	9.84	9.88	8.82	11.35	9.41	9.75	9.09	11.02	10.54	9.46
3.01	3.70	3.36	3.28	3.12	3.36	3.03	3.31	3.20	3.16	3.71	3.30	2.54	2.44	2.90	2.99	2.46
7.63	9.09	8.37	9.22	8.19	8.38	7.88	8.35	7.30	7.95	9.05	7.28	8.98	7.71	10.50	9.63	9.09
1.25	1.48	1.40	1.37	1.38	1.36	1.22	1.35	1.18	1.34	1.44	1.21	1.40	1.28	1.50	1.48	1.44
6.97	8.51	7.46	7.71	7.49	7.50	6.85	7.71	6.88	7.67	7.97	7.31	8.27	6.98	8.62	8.35	8.67
1.37	1.72	1.53	1.53	1.59	1.52	1.39	1.54	1.40	1.52	1.74	1.44	1.55	1.45	1.64	1.66	1.53
3.65	4.26	3.92	4.28	4.16	3.88	3.73	4.39	3.83	3.62	4.55	3.72	4.40	3.72	4.49	4.28	4.22
0.51	0.61	0.55	0.59	0.56	0.56	0.54	0.55	0.51	0.52	0.64	0.53	0.56	0.54	0.61	0.57	0.57
2.90	3.65	3.45	3.64	3.47	3.57	3.41	3.45	3.20	3.46	3.84	3.13	3.63	3.21	3.75	3.40	3.72
0.48	0.61	0.53	0.60	0.55	0.56	0.54	0.53	0.50	0.54	0.58	0.48	0.57	0.52	0.58	0.56	0.56
6.33	7.67	6.82	6.70	6.51	6.49	6.38	6.16	6.52	6.84	6.85	6.17	7.87	6.42	8.69	8.14	6.93
1.41	1.72	1.48	1.53	1.50	1.51	1.54	1.41	1.47	1.52	1.56	1.37	2.08	1.82	2.36	2.17	1.74
5.46	6.65	8.82	6.63	5.56	6.70	6.14	4.98	4.75	5.31	7.82	5.49	6.92	4.66	6.24	5.62	5.73
3.16	3.69	3.41	3.38	2.95	2.97	3.18	3.07	2.88	2.99	3.70	3.04	4.88	3.31	3.84	3.99	4.14
0.84	0.94	0.99	0.87	0.85	0.76	0.71	0.69	0.62	0.73	0.93	0.55	0.99	0.82	0.86	0.92	0.99

(2004). Analytical precision was generally better than 2% for most oxides and better than 1% for SiO_2. Trace elements were also analyzed at the University of Hong Kong by ICP-MS using the procedures described in Qi et al. (2000). Powdered samples of ~50 mg were dissolved in high-pressure Teflon bombs using a $HF–HNO_3$ mixture. An internal standard solution containing the single element Rh was used to monitor signal drift during ion counting. Analytical precision for most elements was better than 5%. The analytical results for major and trace elements are listed in Table 1.

4.3. Whole-rock Sr–Nd–Pb isotope analyses

Sr–Nd and Pb isotopes were measured with a Finnigan MAT 262 thermal ionization mass spectrometer at the Institute of Geology and Geophysics, Chinese Academy of Sciences, Beijing. Analytical procedures are available in Zhang et al. (2001). Measured $^{87}Sr/^{86}Sr$ and $^{143}Nd/^{144}Nd$ ratios were normalized to $^{86}Sr/^{88}Sr = 0.1194$ and $^{146}Nd/^{144}Nd = 0.7219$, respectively. The reported $^{87}Sr/^{86}Sr$ and $^{143}Nd/^{144}Nd$ ratios were adjusted to the NBS SRM 987 standard $^{87}Sr/^{86}Sr = 0.71025$ and the Shin Etsu JNdi-1 standard $^{143}Nd/^{144}Nd = 0.512115$. Sr–Nd isotope results are listed in Table 2.

Pb was separated by anion exchange techniques with diluted HBr as an eluant. Repeated analyses of standard NBS 981 yielded $^{204}Pb/^{206}Pb = 0.05897 \pm 15$, $^{207}Pb/^{206}Pb = 0.91445 \pm 80$, and $^{208}Pb/^{206}Pb = 2.16170 \pm 180$. Data for selected samples are also listed in Table 3.

5. Analytical results

5.1. Mineral compositions

Representative analyses of olivine phenocrysts from the ultramafic dyke show relatively high MgO, with Fo values ranging from 70 to 85. Most grains are zoned with a Mg-rich core and a more Fe-

Table 2
Sr–Nd isotopes for the basaltic flows and mafic–ultramafic dykes from the Tarim Basin, SW China.

Sample	Rb (ppm)	Sr (ppm)	$^{87}Rb/^{86}Sr$	$^{87}Sr/^{86}Sr$	(2σ)	$^{87}Sr/^{86}Sri$	Sm (ppm)	Nd (ppm)	$^{147}Sm/^{144}Nd$	$^{143}Nd/^{144}Nd$	(2σ)	$^{143}Nd/^{144}Ndi$	εNd
Basaltic flow													
AQI-2	20.6	432	0.1384	0.707671	0.000009	0.70713	9.39	42.6	0.1334	0.512388	0.000014	0.512149	−2.66
AQII-3	17.7	439	0.1165	0.707453	0.000006	0.70700	9.75	45.0	0.1311	0.512217	0.000017	0.511982	−5.92
AQIII-3	22.1	395	0.1617	0.707017	0.000010	0.70639	12.06	55.9	0.1306	0.512204	0.000057	0.511970	−6.16
AQIII-8	23.1	592	0.1128	0.707605	0.000013	0.70717	9.01	41.0	0.1330	0.512130	0.000017	0.511892	−7.68
AQIV-2	18.8	410	0.1328	0.707663	0.000008	0.70715	9.09	42.7	0.1287	0.512159	0.000038	0.511928	−6.97
AQV-2	17.3	1112	0.0450	0.708210	0.000020	0.70803	10.78	51.3	0.1270	0.512164	0.000022	0.511936	−6.82
AQVI-2	21.5	416	0.1492	0.707167	0.000006	0.70659	8.88	41.2	0.1303	0.512336	0.000020	0.512102	−3.57
AQVII-2	26.9	1114	0.0698	0.707641	0.000012	0.70737	9.81	45.7	0.1299	0.512349	0.000006	0.512116	−3.31
AQVIII-2	26.0	426	0.1771	0.708647	0.000010	0.70796	9.37	41.5	0.1364	0.512055	0.000043	0.511810	−9.27
AQVIII-8	20.0	355	0.1630	0.708080	0.000016	0.70744	8.78	39.8	0.1333	0.512275	0.000037	0.512036	−4.86
Mafic dyke													
XH2-36	46.4	712	0.1882	0.705553	0.000014	0.70482	11.65	57.0	0.1237	0.512771	0.000007	0.512549	5.16
XH2-54	19.0	473	0.1159	0.705605	0.000010	0.70515	10.23	46.9	0.1319	0.512606	0.000005	0.512369	1.64
Ultramafic dyke													
XH2-62	8.4	193	0.1263	0.705329	0.000023	0.70484	3.67	15.8	0.1406	0.512683	0.000007	0.512431	2.85

rich rim (Fig. 4). The analyzed clinopyroxene is augite and diopside ($En_{40-54}Fs_{9-14}Wo_{36-47}$) with TiO_2 contents ranging from 0.34 to 1.68 wt.% and Al_2O_3 from 1.87 to 4.48 wt.%.

5.2. Major and trace elements

5.2.1. Basaltic flows

The basalts have relatively homogeneous bulk-rock compositions (Fig. 5). Their SiO_2 contents range from 44.1 to 50.0 wt.%, Al_2O_3 from 14.2 to 17.4 wt.%, and MgO from 2.1 to 7.1 wt.% (normalized to 100% anhydrous). They have high Fe_2O_{3T} (12.6–17.0 wt.%) with corresponding Mg/(Mg + Fe) ratios of 0.41–0.48. Their TiO_2 contents are also relatively high (3.53–4.33 wt.%) (Fig. 5). They are highly alkalic with Na_2O ranging from 2.64 to 5.41 wt.% and K_2O from 0.90 to 2.44 wt.% with Na_2O/K_2O ratios of 1.5–4.0. They fall in the alkaline series in the plots of SiO_2 vs. $Na_2O + K_2O$ and Nb/Y vs. Zr/TiO_2 (Fig. 5a, b) (Winchester and Floyd, 1977; Le Bas et al., 1986).

The basalts have uniform chondrite-normalized REE patterns enriched in LREE with slightly negative to positive Eu anomalies (Eu/Eu* = 0.78–1.71) (Fig. 6a). They have $(La/Yb)_N$ (primitive mantle normalized) ratios ranging from 6.7 to 10.7 and $(La/Sm)_N$ from 2.1 to 3.2. In the primitive mantle-normalized diagram (Fig. 7a), the basalts have patterns enriched in LILE (Rb, Ba, Th and U) with slightly negative Nb and Ta anomalies. In general, the basalts have patterns similar to those of ocean island basalts (OIB) (Fig. 7a).

5.2.2. Mafic and ultramafic dykes

The mafic dykes are somewhat more evolved than the basalts with SiO_2 = 47.3–55.5 wt.%, Al_2O_3 = 13.7–17.0 wt.%, Fe_2O_3 = 9.15–14.9 wt.%, CaO = 5.15–9.89 wt.%) and $K_2O + Na_2O$ = 3.20–7.79 wt.%. These mafic dykes have lower TiO_2 contents (<3.5 wt.%) than the basalts but still plot in the alkaline field (Fig. 5). Four samples from an ultramafic dyke have significantly higher MgO (19.0–20.3 wt.%) and lower TiO_2 than the basalts. They have lower Al_2O_3 (6.5–6.9 wt.%) and $Na_2O + K_2O$ (0.91–1.03 wt.%) and therefore plot in the calc-alkaline field (Fig. 5).

The mafic dykes display chondrite-normalized REE patterns enriched in LREE with $(La/Yb)_N$ ranging from 10.8 to 14.4 and $(La/Sm)_N$ from 2.5 to 3.46 (Fig. 6b). Rocks from the ultramafic dyke have much lower total REE abundances (72–78 ppm) than the mafic dykes (182–310 ppm) but both have similar patterns and are characterized by relatively low $(La/Yb)_N$ (8.7–8.9) and $(La/Sm)_N$ (2.0–2.1) ratios. Both mafic and ultramafic dykes lack obvious Eu anomalies (Fig. 6b). In the primitive mantle-normalized trace element diagram (Fig. 7b), the mafic dykes show enrichment in LILE and HFSE similar to that of OIB, but the ultramafic samples have lower trace element concentrations compared to the mafic dykes (Fig. 7b).

Table 3
Pb–Pb isotopes for the basaltic flows and mafic–ultramafic dykes from the Tarim Basin, SW China.

	$^{206}Pb/^{204}Pb$	(2σ)	$^{207}Pb/^{204}Pb$	(2σ)	$^{208}Pb/^{204}Pb$	(2σ)
Basaltic flow						
AQ1-2	17.9950	0.0009	15.5798	0.0008	38.6583	0.0022
AQ2-3	17.9289	0.0008	15.5348	0.0007	38.5062	0.0017
AQ3-3	18.0217	0.0007	15.5459	0.0008	38.5519	0.0028
AQ3-8	18.0304	0.0013	15.5809	0.0010	38.6346	0.0024
AQ4-2	17.9327	0.0012	15.5264	0.0011	38.4922	0.0034
AQ5-2	17.9008	0.0004	15.5182	0.0003	38.5034	0.0007
AQ6-2	17.9971	0.0004	15.5265	0.0004	38.5106	0.0010
AQ7-2	17.8719	0.0008	15.5179	0.0008	38.3789	0.0018
AQ8-2	17.9080	0.0007	15.5333	0.0006	38.5086	0.0014
AQ8-8	17.9578	0.0007	15.5164	0.0007	38.4329	0.0018
Mafic dyke						
XHZ-36	18.0058	0.0007	15.5772	0.0006	38.4253	0.0015
XHZ-54	18.7680	0.0005	15.5402	0.0004	39.0445	0.0009
Ultramafic dyke						
XHZ-62	18.6850	0.0013	15.5504	0.0013	38.9553	0.0040

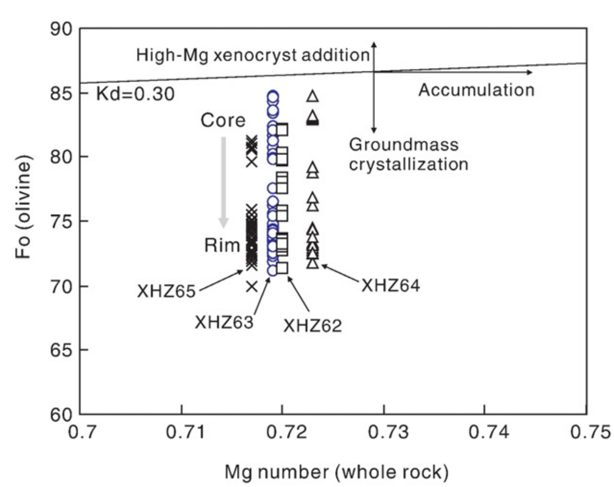

Fig. 4. Mg-number of olivine versus Mg-number of the whole rocks from samples of the ultramafic dyke in Bachu, Western Tarim Basin.

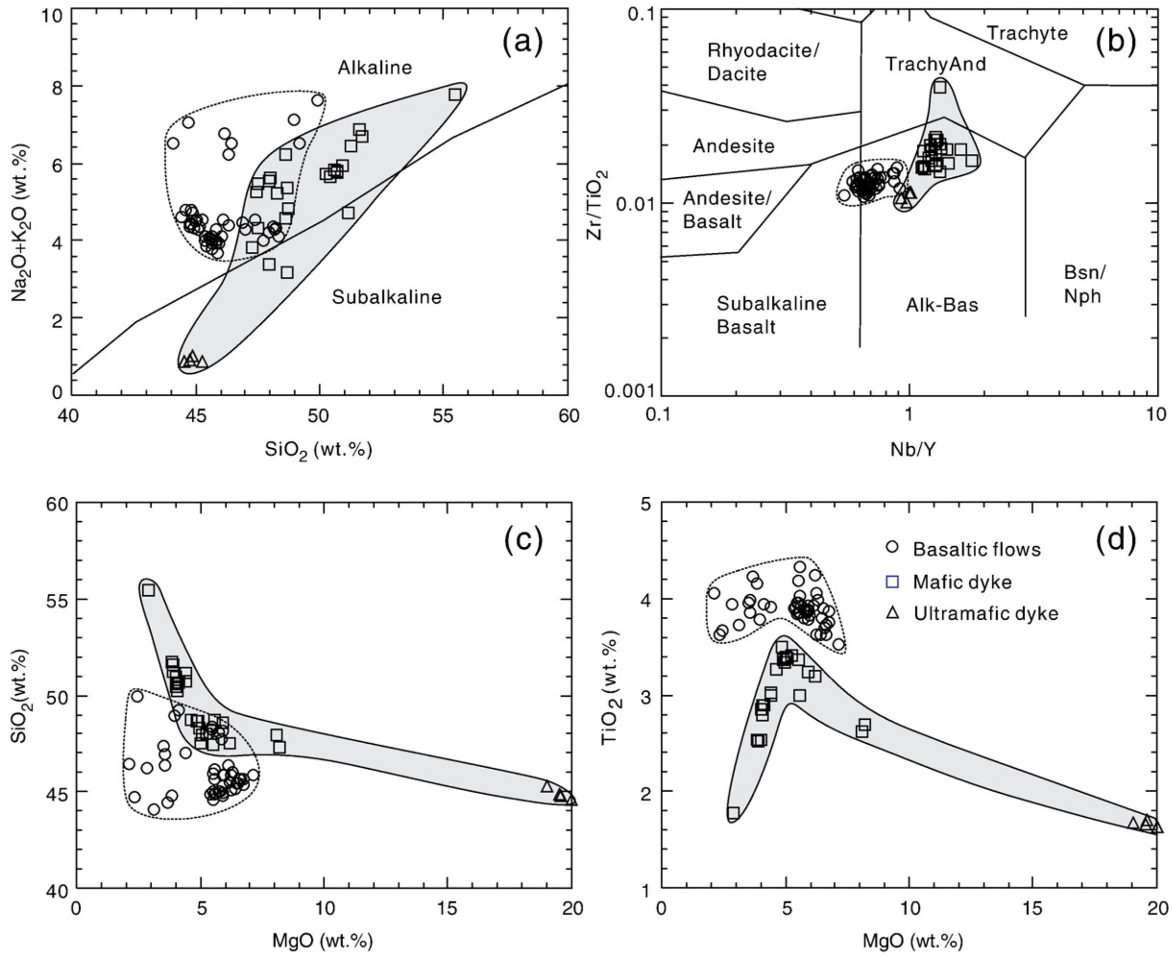

Fig. 5. Plots of SiO_2 vs. Na_2O+K_2O, Nb/Y vs. Zr/TiO_2, MgO vs. SiO_2 and MgO vs. TiO_2 for the basalts and dykes in the Tarim Basin. The discrimination diagrams are from Le Bas et al. (1986) and Winchester and Floyd (1977), respectively.

5.3. Sr–Nd–Pb isotopes

The basalts display a wide range of isotope compositions (Table 2) with initial $^{87}Sr/^{86}Sr$ ratios ranging from 0.7064 to 0.7080 and $^{143}Nd/^{144}Nd$ ratios from 0.51181 to 0.51215 (Fig. 8). The corresponding εNd(t) values range from −2.7 to −9.3. The basalts all have very uniform ratios of $^{206}Pb/^{204}Pb$ (17.87–18.03), $^{207}Pb/^{204}Pb$ (15.52–15.58) and $^{208}Pb/^{204}Pb$ (38.38–38.66) (Table 3). The samples plot above the Northern Hemisphere Reference Line (NHRL) and near to the EM1 end-member (Fig. 9).

Two analyzed samples of the mafic dykes have slightly lower initial $^{87}Sr/^{86}Sr$ (0.7048 to 0.7052) and slightly higher initial $^{143}Nd/^{144}Nd$ ratios (0.51237 to 0.51255) than the basalts (Fig. 8). The dykes have positive εNd(t) values of +1.64 to +5.16. These dykes also have relatively uniform ratios of $^{206}Pb/^{204}Pb$ (18.01–18.77), $^{207}Pb/^{204}Pb$ (15.54–15.58) and $^{208}Pb/^{204}Pb$ (38.43–39.04) (Fig. 9). One sample from the ultramafic dyke has intermediate ratios of $^{87}Sr/^{86}Sr$ (0.7048) and a εNd(t) value of +2.9. The Pb isotopes of this sample, $^{206}Pb/^{204}Pb=18.69$, $^{207}Pb/^{204}Pb=15.55$ and $^{208}Pb/^{204}Pb=38.96$, are comparable with those of the mafic dykes (Figs. 8 and 9).

6. Discussion

6.1. Magma differentiation and crustal contamination

In general, samples from the mafic dykes show linear correlations between major elements and MgO. Plots of TiO_2 and Fe_2O_3 vs. MgO display convex patterns for both analyzed dykes (Fig. 5), indicating fractional crystallization of Fe–Ti oxides during the late stages of magma evolution. The absence of Sr and Eu anomalies in the trace element plots suggests that plagioclase was not a major fractionating phase (Fig. 6). Rocks from the ultramafic dyke have relatively high MgO and low Al_2O_3 and total alkalis (Fig. 5), consistent with accumulation of olivine and clinopyroxene. Analyses of representative olivine cores and margins are shown in the plot of Fo values versus whole-rock Mg-numbers (Fig. 4). All of the phenocryst cores plot to the right of the equilibrium curve, which is defined on the assumption that the value of K_D for distribution of Fe^{2+} and Mg between olivine and melt is 0.3 (Ulmer, 1989). Such relationships result from olivine accumulation, consistent with the mineral assemblages, in which large, subhedral olivine crystals make up more than 50% of the rock. Ultramafic dyke samples have relatively high Cr (1070 to 1140 ppm) and Ni (560 to 602 ppm), and lack Eu anomalies in their chondrite-normalized REE patterns (Fig. 6b), again suggesting accumulation of mafic minerals. However, both the mafic and ultramafic dykes have similar isotopic compositions and some element ratios. It is therefore likely that both the mafic and ultramafic dykes formed from a common magma.

Although they have similar major element contents, the basaltic flows and dykes follow different evolution trends (Fig. 5). In particular, the basaltic flows have TiO_2 contents higher and Zr/TiO_2 and Nb/Y ratios lower than the dykes. These differences indicate that they were derived from different magmas.

Both the mafic and ultramafic dykes have relatively constant whole-rock Sr–Nd isotopes and do not show strong crustal contamination (Fig. 8). There are no Nb, Ta, P, and Ti anomalies on the trace-element patterns (Fig. 7b), indicative of insignificant contamination. Some samples

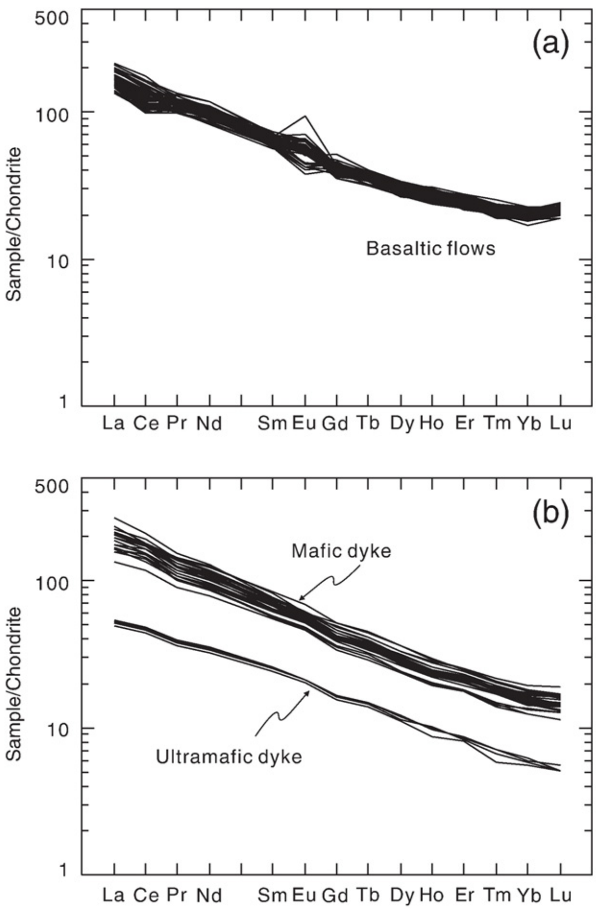

Fig. 6. Chondrite-normalized patterns for the basalts and dykes in the Tarim Basin. The normalized values are from Sun and McDonough (1989).

from the mafic dykes have positive Pb anomalies on the primitive mantle normalized trace element patterns (Fig. 7b). These anomalies may be due to analytical error or reflect selective Pb contamination.

Although the basaltic flows have OIB-like trace element patterns (Fig. 7a), their slightly negative Nb and Ta anomalies are indicative of minor crustal contamination. Lu and Yb have similar geochemical characters and Lu/Yb ratios cannot be significantly modified by partial melting or fractional crystallization. Mantle-derived magmas are characterized by low Lu/Yb ratios (0.14–0.15) (Sun and McDonough, 1989), whereas continental crust has relatively higher Lu/Yb ratios (0.16–0.18). In addition, the continental crust is rich in LREE and LILE but strongly depleted in Nb and Ta (Rollinson, 1993; Rudnick and Gao, 2003). The basaltic flows have somewhat variable, but generally high, Lu/Yb ratios (0.14–0.17) and low Nb/La ratios (0.59–0.89) (Fig. 10a), clearly suggesting some crustal contamination. Crustal contamination is also evidenced by the slightly elevated Rb/La and Pb/Nb ratios of these rocks (Fig. 10b).

The basalts have relatively high initial $^{87}Sr/^{86}Sr$ ratios (0.7064 to 0.7080) and variably low εNd values (−2.66 to −9.27) (Table 2). The large scatter of both $^{87}Sr/^{86}Sr$ ratios and εNd values is consistent with variable degrees of crustal contamination (Fig. 8). Samples with high $^{87}Sr/^{86}Sr$ ratios and low εNd values have higher Th/Nb ratios (0.1–0.16), clearly demonstrating the involvement of crustal assimilation. In the plot of initial $^{143}Nd/^{144}Nd$ values versus initial $^{87}Sr/^{86}Sr$ ratios, the basalts lie between the enriched extension of the "mantle array" defined by mantle-derived rocks and crustal rocks (Fig. 8), suggesting variable degrees of crustal contamination during magma ascent and differentiation. It is reasonable to assume that primitive magmas may have isotope compositions similar to sample AQ12 with the highest whole rock εNd(t) values among the basalts. Using both the Archean amphibolite and felsic gneiss in the northern margin of the Tarim Block as the basement through which the magmas passed, modeling shows that the samples with low εNd(t) values may have undergone variable degrees (up to 10%) of felsic crustal contamination (Fig. 8). Samples with relatively high Sm/Nd ratios may be due to the contamination by minor mafic crust.

6.2. OIB-like, heterogeneous mantle sources

The mafic and ultramafic dykes in Bachu belong to the alkaline series with high Nb/Y ratios (0.55–1.78) (Fig. 5). The dykes do not show crustal contamination and display OIB-like trace element patterns with enrichment of large-ion lithophile elements (LILE), high field strength elements (HFSE) and LREE (Fig. 6). In the primitive mantle-normalized diagram, they do not show obvious negative Nb, Ta and Ti anomalies, typical of OIB (Fig. 7a and b). Their low ($^{87}Sr/^{86}Sr$)i ratios (0.7048 to 0.7052) and positive εNd(t) values (+1.64 to +5.16) indicate a mantle source that was enriched relative to the bulk Earth (Sun and McDonough, 1989). This type of mantle source is similar to that of many primary oceanic and continental alkaline suites that have positive εNd(t) in association with LREE enrichment, evidence for an OIB-like, asthenospheric mantle source.

The basaltic flows in Keping also belong to the alkaline series with high Nb/Y ratios (0.55–1.78) (Fig. 5). Their trace element patterns are again similar to OIB (Figs. 7 and 10; McDonough et al., 1985). Although these flows have undergone variable crustal contamination, the enrichment of LILE and HFSE and the steep chondrite-normalized LREE patterns of the basaltic rocks cannot be explained by crustal assimilation, because the rocks have even higher REE than normal

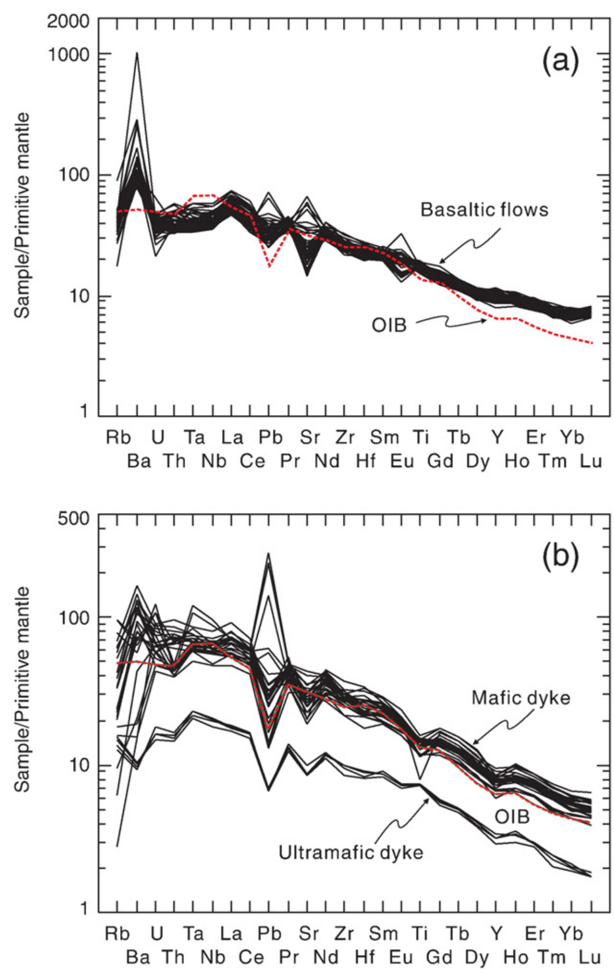

Fig. 7. Primitive mantle-normalized trace element patterns for the basalts and dykes in the Tarim Basin. The normalizing values are from Sun and McDonough (1989).

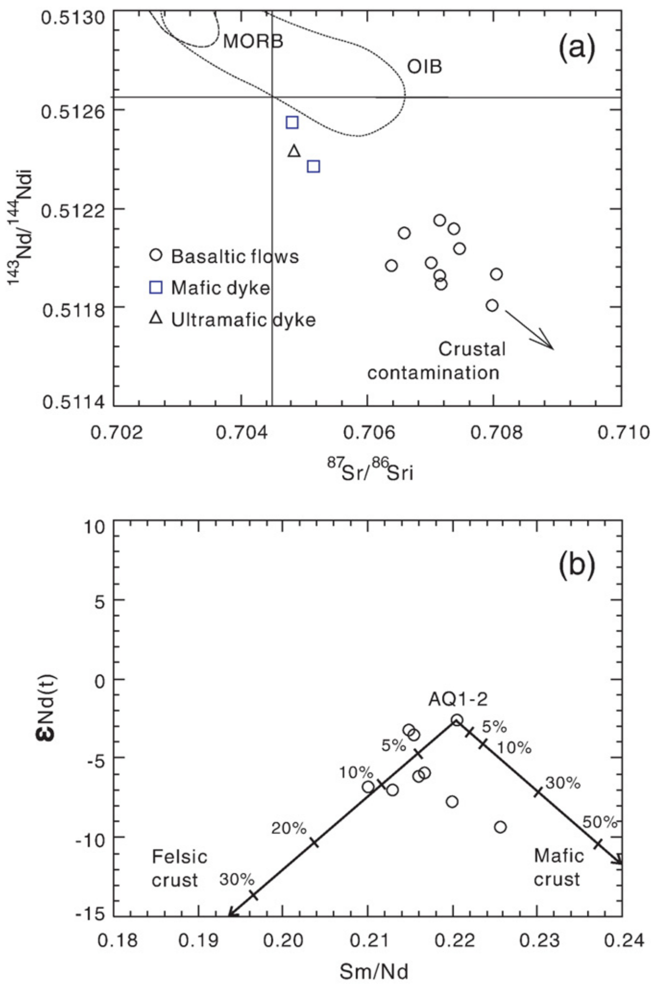

Fig. 8. a. Initial $^{87}Sr/^{86}Sr$ vs. $^{147}Nd/^{144}Nd$ ratios for the basalts and dikes from the Tarim Basin. MORB (Wilson, 1989), OIB (Staudigel et al., 1984) and the Emeishan basalts (Wang et al., 2007) are also shown for comparison. b. Plot of Sm/Nd versus $\varepsilon Nd(t)$ to show variable degrees of crustal contamination, using sample AQ1–2 (Sm/Nd = 0.22, $\varepsilon Nd(t) = -2.66$) as the original magma and the Archean felsic gneiss (Sm/Nd = 0.16, $\varepsilon Nd(t) = -30$) and amphibolite (Sm/Nd = 0.25, −20.25) along the northern margin of the Tarim Block as contaminants (Hu et al., 1997).

crustal materials which are depleted in Nb and Ta (Rudnick and Gao, 2003). Such an enrichment of LILE, HFSE, and LREE is most likely a primary feature indicative of an OIB-like mantle source. The relatively high Sr isotope ratios and negative $\varepsilon Nd(t)$ values (−2.66 to −9.27) of the basaltic flows can be a combination of an enriched mantle source and variable degrees of crustal contamination. We suggest that the basaltic flows were derived from an OIB-like mantle source which was isotopically more enriched than the source of the dykes.

Plots of Zr/Y and $(La/Sm)_N$ ratios are widely used to examine the nature of the mantle source because they do not vary during the magma evolution (Gurenko et al., 2006). These plots clearly demonstrate that the basaltic flows from Keping were probably derived from a mantle source containing 2% garnet and 2% spinel, whereas the mafic and ultramafic dykes were generated by melting of a mantle source containing 5% garnet + 4% amphibole + 1% phlogopite (Fig. 11).

6.3. Mantle plume origin and implication for a large igneous province

Recent geochronological and stratigraphic studies of the Permian basalts in Tarim and the surrounding areas show that a large volume of basalt was erupted between 280 and 270 Ma (Fig. 1) (Chen et al., 1997, 1999; Jia et al., 2004; Jiang et al., 2004a; Chen et al., 2006; Zhou et al., 2006). Paleontological data and stratigraphic correlations suggest that the Kupukuziman and Kaipaizileike Formations are lower to middle and middle Permian, respectively (Zhang, 2003). Previous age data obtained for the Permian basalts and plutonic rocks include K–Ar, ^{40}Ar–^{39}Ar and zircon SHRIMP U–Pb ages for basalts, diabases and syenite, respectively, from the northwestern and southwestern parts of the Tarim Basin. For example, ^{40}Ar–^{39}Ar dating of whole-rock basalts from Keping yielded a plateau age of 281.8 ± 4.2 Ma (2σ) (Yang et al., 2006a), and a recent zircon SHRIMP date on the Xiaohaizi syenite yielded an age of 277 Ma (Yang et al., 2007). Zhang et al. (2008) reported an age of 274 Ma for a syenite intrusion and Yang et al. (1996) obtained a plateau ^{40}Ar–^{39}Ar age of 278 ± 1.4 Ma for the Kupukuziman Formation in Sishichang and an ^{40}Ar–^{39}Ar age of 278 ± 1 Ma for the Xiaohaizi syenite. Thus, these volcanic and plutonic rocks were likely contemporaneous and formed at ~275 Ma (Zhang et al., 2008).

It is commonly believed that the Tarim Block was amalgamated to the Central Asian Orogenic Belt in the Late Carboniferous when the Paleo-Asian ocean was closed because ophiolites younger than Late Carboniferous are not known in the region (Shu et al., 2000; Xia et al., 2003; Li, 2006). Despite this evidence, Yang et al. (1996, 2005, 2006a,b) proposed that the Permian igneous event in the Tarim region was related to northward subduction of the paleo-Tethyan oceanic lithosphere as documented in Xiao et al. (2002, 2005). However, a subduction zone origin for the Tarim mafic and ultramafic rocks is not supported by either

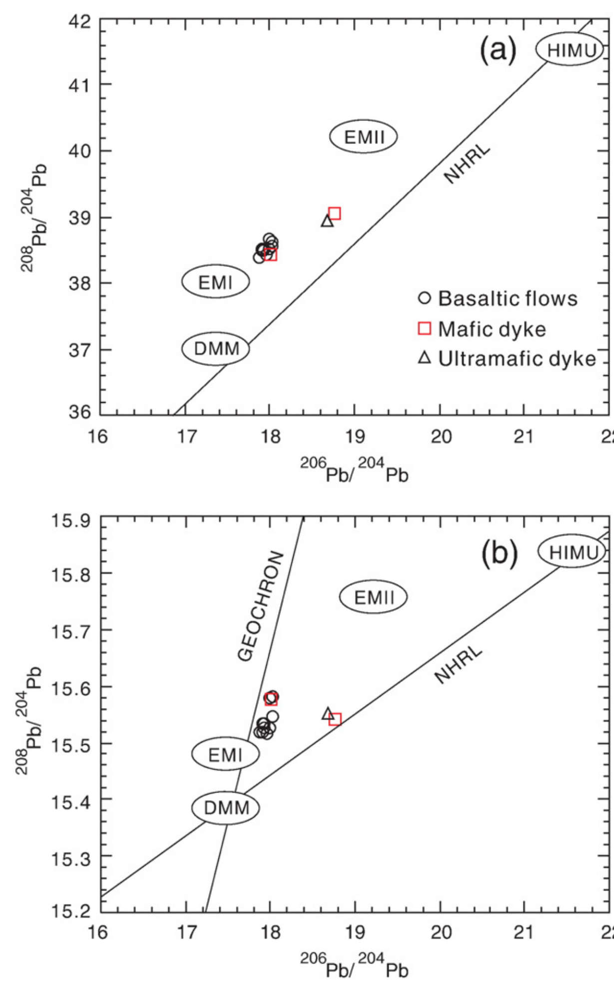

Fig. 9. Plots of $^{206}Pb/^{204}Pb$ vs. $^{208}Pb/^{204}Pb$ and $^{206}Pb/^{204}Pb$ vs. $^{207}Pb/^{204}Pb$ for the basalts and dykes in the Tarim Basin. The fields of HIMU, DMM, EM1 and EM2 are from Zindler and Hart (1986) and Weaver (1991). Northern Hemisphere Reference Line (NHRL) is from Hart (1984).

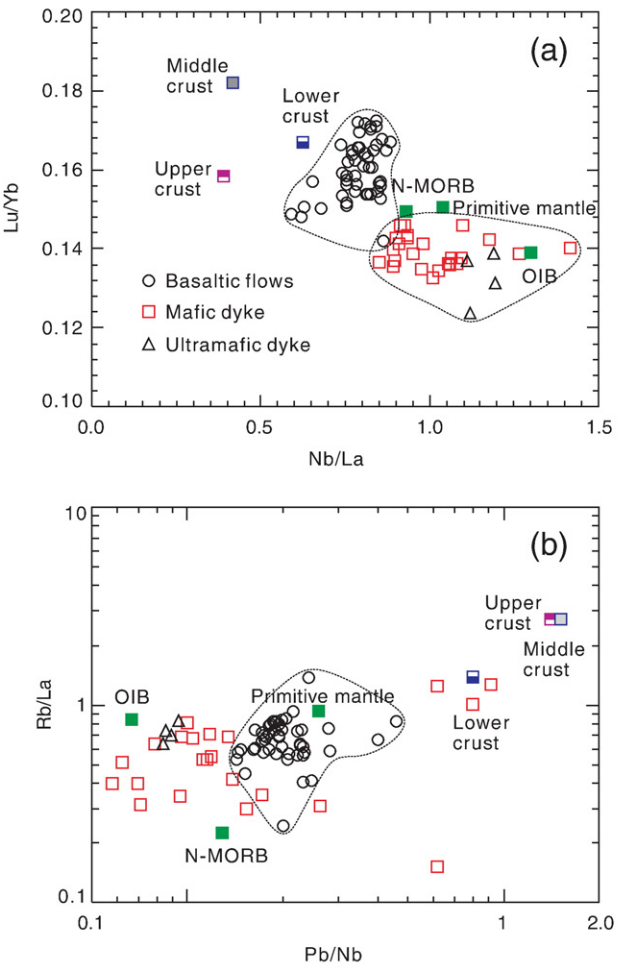

Fig. 10. Plots of Nb/La vs. Lu/Yb and Pb/Nb vs. Rb/La for the basalts and dykes from the Tarim Basin. The upper-, middle- and lower crust are from Rudnick and Gao (2003). OIB, primitive mantle and N-MORB are from Sun and McDonough (1989).

their wide distribution or their geochemistry. Subduction-related mafic rocks typically occur in linear belts and are usually characterized by strongly negative Nb–Ta and Zr–Hf anomalies. The mafic and ultramafic dykes in Tarim do not show such anomalies. Despite variable degrees of crustal contamination, the basaltic flows have only slightly negative Nb–Ta and slightly positive Zr–Hf anomalies, which argue strongly against a subduction-related origin.

Although it is possible that the magmatism may be linked to post-orogenic extension (Zhou et al., 2006), the source of heat required for melting remains un-explained. We agree that the Permian volcanic rocks are more likely related to a mantle plume as proposed recently by various authors (Jiang et al., 2004a,b, 2006b; Zhang et al., 2008). The diversity of Siberia Traps and ELIP basalts has been explained as products of heterogeneous asthenospheric mantle sources (e.g. Arndt et al., 1998; Zhou et al., 2008). High temperatures required for melting of such asthenospheric mantle can be provided by a mantle plume. In the Bachu area, temporally and spatially associated syenitic intrusions have A-type granite affinities (Zhang et al., 2008). These type of intrusions are widely recognized as a feature of the ELIP in SW China, which is believed to have been derived from a mantle plume (Shellnutt and Zhou, 2007).

Olivine from the ultramafic dyke has much higher CaO contents (0.21 to 0.61 wt.%) than that of olivine in mantle xenoliths (Thompson and Gibson, 2000) and may have been crystallized from a high-Mg magma with a picritic composition. The most Mg-rich olivine core (Fo_{85} in sample XHZ63) corresponds to olivine that crystallized from relatively primary mantle-derived melts. Assuming a $K_D(\text{Fe–Mg})^{\text{ol-liq}}$ of 0.30 ± 0.03 (Ulmer, 1989), olivine with Fo_{85} would have been in equilibrium with a parental magma having a minimum Mg# (atomic Mg/Fe + Mg) of 0.63. If a $K_D(\text{Fe–Mg})^{\text{ol-liq}}$ of 0.35 is used, which is the mean value of magmas equilibrated at pressures of >2.3 GPa (Putirka, 2005), a higher Mg# of 0.67 is obtained.

The relationship between the composition of olivine and liquidus temperature of basaltic melts has been well-established by experimental results and phase equilibrium analyses (Roeder and Emslie, 1970; Weaver and Langmuir, 1990; Grove et al., 1992). The following formula can be used to estimate the liquidus temperatures of olivine and basalts:

$$T_{\text{liquidus}}(^{\circ}\text{C}) = 1066 + 12.067\text{Mg\#} + 312.3(\text{Mg\#})^2.$$

According to the highest Fo values (85) of olivine from the ultramafic dyke at Bachu, the liquidus temperature of olivine was as high as 1303 °C, and the corresponding liquidus temperature of the basaltic melts was 1200 °C ($K_D = 0.30 \pm 0.03$). Such high-Mg parental magmas with a high temperature further suggest that the magmas were generated from an upwelling mantle plume.

Permian igneous rocks are not only present in the Tarim Basin but are widespread in NW China. For example, many mafic–ultramafic intrusions occur in the Huangshan district of the eastern Tianshan Mountains (Zhou et al., 2004, Chai et al., 2008). The Huangshan intrusions also contain high-Mg olivine (Fo = 82–89) and thus had high-Mg parental magmas (minimum Mg# values of 73) with high melting temperatures (Zhou et al., 2004). These intrusions have been dated at ~270 Ma and are thought to have been derived from a mantle plume but show strong interaction with a subduction-modified lithospheric mantle (Zhou et al., 2004). Basalts in the Turpan-Hami and Sangtanghu basins of north Tienshan and Liuyuan of East Tianshan are also likely to have been derived from a Permian mantle plume (Zhou et al., 2006, Fig. 1a). Voluminous Permian igneous rocks also occur in the adjacent Hongliuhe and Beishan areas to the east (Yang et al., 2005). Thus, it is possible that the coeval mafic rocks in Tarim and the surrounding regions constitute a Permian LIP in NW China. This LIP may also include some of the A-type granites in the Central Asian Orogenic Belt. These A-type granites with positive εNd (t) values are well-known to be coeval with Permian mafic rocks (Jahn et al., 2000a,b; Pirajno et al., 2008).

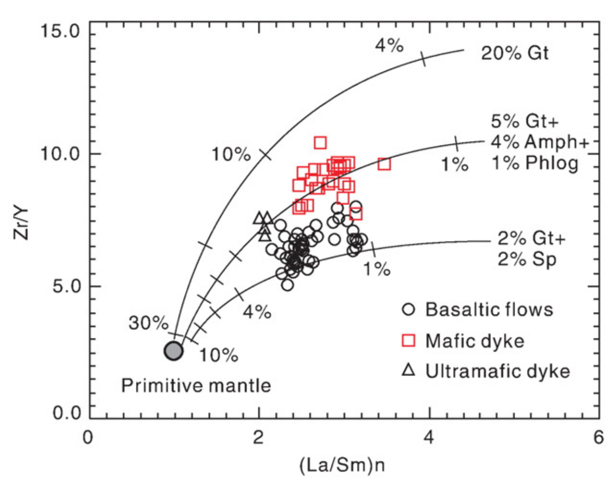

Fig. 11. Plot of (La/Sm)n vs. Zr/Y for the basalts and dykes from the Tarim Basin. Solid lines represent melt compositions resulting from batch melting of peridotite corresponding in composition to primitive mantle (Gurenko et al., 2006). This figure demonstrates the effect of source mineral composition on the variation of Zr/Y ratios in the whole rocks but does not quantitatively constrain the degree of partial melting. Gr—garnet, Amph—amphibole, Phlog—phlogopite, Sp—spinel.

Yang et al. (1996) and Chen et al. (1997) suggest that the Tarim Basin experienced a major tectonothermal event in the Permian, with strong imprints in the central and western parts of the basin. This interpretation is supported by the presence of the voluminous igneous rocks formed in an intraplate environment. Other Permian thermal events have also been identified in NW China. For example, Shu et al. (2000) reported $^{40}Ar/^{39}Ar$ ages of 269 Ma for muscovite and 281 Ma for biotite in a deformed granite in the Weiya area of eastern Tianshan. We suggest that the large-scale Permian igneous activity in NW China can be attributed to mantle plume activity, although it is unknown if a single plume or several plumes were involved (Borisenko et al., 2006; Pirajno et al., 2009). Indeed, Middle and Late Permian mantle plumes were very active in the Eurasian continent, as evidenced by the well-known ~250 Ma Siberian Traps and the ~260 Ma Emeishan LIP. Latest Permian volcanic ashes also occur widely across Eurasia (Yin et al., 1992). The wide distribution and the range of ages of these Permian plumes in Eurasia (Tarim LIP, ELIP and Siberian Traps) may suggest a single protracted thermal anomaly caused by heat loss from the core, which may have contributed collectively to the Permian mass extinction.

7. Conclusions

Basaltic flows interlayered with Middle Permian sedimentary rocks in the Keping area and mafic and ultramafic dykes in the Bachu area of the western Tarim Basin were derived from OIB-like, asthenospheric, isotopically heterogeneous mantle sources. The high-temperature and high-Mg nature of the parental magmas suggest a mantle plume origin. This mantle plume may have produced the basalts and the coeval mafic intrusions in the Tarim Basin and surrounding regions, thus forming the ~275 Ma Tarim LIP.

Acknowledgments

This work was supported by a grant from the Research Grant Council of Hong Kong (HKU7058/08P), a project from the State Key Laboratory of Ore Deposit Geochemistry, Institute of Geochemistry, CAS (200802), a CVRD-INCO research grant and a Chinese 973 Project matching grant from HKU (to MFZ). Field work in 2007 was assisted by the local geological teams of Xinjiang and Yang Yang. We are sincerely thankful to Peter C. Lightfoot for his support over the years and for initiating this research project and to Paul T. Robinson for his great help during the preparation of this paper. Official reviews by Franco Pirajno and Marc Reichow and editorial handling by Andrew Kerr are gratefully acknowledged.

References

Arndt, N.T., Chauvel, C., Fedorenko, V., Czamanske, G., 1998. Two mantle sources, two plumbing systems: tholeiitic and alkaline magmatism of the Maymecha River basin, Siberian flood volcanic province. Contributions to Mineralogy and Petrology 133, 297–313.

Borisenko, A.S., Sotnikov, V.I., Izokh, A.E., Polyakov, G.V., Obolensky, A.A., 2006. Permo-Triassic mineralization in Asia and its relation to plume magmatism. Russian Geology and Geophysics 47, 166–182.

Campbell, I.H., Czamanske, G.K., Fedorenko, V.A., Hill, R.I., Stepanov, V., 1992. Synchronism of the Siberian Traps and the Permian-Triassic boundary. Science 258, 1760–1763.

Chai, F.M., Zhang, Z.C., Mao, J.W., Dong, L.H., Zhang, Z.H., Wu, H., 2008. Geology, petrology and geochemistry of the Baishiquan Ni–Cu-bearing mafic–ultramafic intrusions in Xinjiang, NW China: implications for tectonics and genesis of ores. Journal of Asian Earth Sciences 32, 218–235.

Chen, H.L., Yang, S.F., Dong, C.W., 1997. The discovery of early Permian basic rock belt in the Tarim basin and its tectonic meaning. Geochemica 26, 77–87 (in Chinese with English abstract).

Chen, H.L., Yang, S.F., Dong, C.W., 1999. Characteristics and geodynamics of the Early Permian igneous rocks in the Tarim Basin. In: Chen, H.H. (Ed.), Studies on collisional orogenic belt. Ocean Press, Beijing, pp. 174–182 (in Chinese).

Chen, H.L., Yang, S.F., Wang, Q.H., Luo, J.C., Jia, C.Z., Wei, G.Q., Li, Z.L., 2006. Sedimentary response to the Early-mid-Permian basaltic magmatism in the Tarim plate. Geologica Sinica Acta 33, 545–552 (in Chinese).

Chung, S.L., Jahn, B.M., 1995. Plume–lithosphere interaction in generation of the Emeishan flood basalts at the Permian-Triassic boundary. Geology 23, 889–892.

Ernst, R.E., Buchan, K.L., 2001. Mantle Plumes: their identification through time. Geological Society of America Special Paper, vol. 352, p. 593.

Ernst, R.E., Buchan, K.L., 2003. Recognizing mantle plumes in the geological record. Annual Reviews of Earth and Planetary Sciences 31, 469–523.

Grove, T.L., Kinzler, R.J., Bryan, W.B., 1992. Fractionation of mid-ocean ridge basalt (MORB). In: Morgan, J.P., Blackman, D.K., Sinton, J.M. (Eds.), Mantle Flow and Melt Generation at Mid-Ocean Ridges. Geophysics Monography, vol. 71. American Geophysics Union, pp. 281–310.

Gurenko, A.A., Hoernle, K.A., Hauff, F., Schmincke, H.U., Han, D., Miura, Y.N., Kaneoka, I., 2006. Major, trace element and Nd–Sr–Pb–O–He–Ar isotope signatures of shield stage lavas from the central and western Canary Islands: Insights into mantle and crustal processes. Chemical Geology 233, 75–112.

Hart, S.R., 1984. A large-scale isotope anomaly in the southern hemisphere mantle. Nature 309, 753–757.

Hu, A.Q., Wang, Z.-G., Tu, G.-Z., 1997. Geological Evolution and Mineralization in the Northern Xingjiang. Science Press, p. 246 (In Chinese).

Jahn, B.M., Wu, F., Chen, B., 2000a. Granitoids of the Central Asian Orogenic Belt and continental growth in the Phanerozoic. Transactions of the Royal Society of Edinburgh. Earth Science 91, 181–193.

Jahn, B.M., Wu, F.Y., Hong, D.W., 2000b. Important crustal growth in the Phanerozoic: isotopic evidence of granitoids from east-central Asia. the proceedings of the Indian Academy of Sciences. Earth and Planetary Sciences 109, 5–20.

Jia, C.Z., 1997. Tectonic characteristics and oil–gas in the Tarim Basin, China. Petroleum Industry Press, Beijing. (in Chinese).

Jia, C.Z., Zhang, S.B., Wu, S.Z., 2004. Stratigraphy of the Tarim Basin and adjacent areas, vol. 2. Science Press, Beijing, p. 513.

Jiang, C.Y., Zhang, P.B., Lu, D.R., Bai, K.Y., 2004a. Petrogenesis and magma source of the ultramafic rocks at Wajilitag region, western Tarim Plate in Xinjiang. Acta Petrologica Sinica 20, 1433–1444 (in Chinese with English abstract).

Jiang, C.Y., Zhang, P.B., Lu, D.R., Bai, K.Y., Wang, Y.P., Tang, S.H., Wang, J.H., Yang, C., 2004b. Petrology, geochemistry and petrogenesis of the Kalpin basalts and their Nd, Sr and Pb isotopic compositions. Geological Review 50, 492–500 (in Chinese with English abstract).

Jiang, C.Y., Jia, C.Z., Li, L.C., Zhang, P.B., Lu, D.R., Bai, K.Y., 2004c. Source of the Fe-enriched-type high-Mg magma in Mazhartag region, Xinjiang. Acta Geologica Sinica 78, 770–780 (in Chinese with English abstract).

Jiang, C.Y., Cheng, S.L., Ye, S.F., Xia, M.Z., Jiang, H.B., Dai, Y.C., 2006a. Lithogeochemistry and petrogenesis of the Zhongposhanbei mafic rock body, at Beishan region, Xinjiang. Acta Petrologica Sinica 22, 115–126.

Jiang, C.Y., Li, Y.Z., Zhang, P.B., Ye, S.F., 2006b. Petrogenesis of Permian basalts on the western margin of the Tarim basin, China. Russian Geology and Geophysics 47, 237–248.

Le Bas, M.J., Le Maitre, R.W., Streckeisen, A., Zanettin, B., 1986. A chemical classification of volcanic rocks based on the total alkali-silica diagram. Journal of Petrology 27, 745–750.

Li, J.Y., 2006. Permian geodynamic setting of northeast China and adjacent regions: closure of the Paleo-Asian Ocean and subduction of the Paleo-Pacific Plate. Journal of Asian Earth Sciences 26, 207–224.

Lightfoot, P.C., Hawkesworth, C.J., Hergt, J., Naldrett, A.J., Gorbachev, N.S., Fedorenko, A., Doherty, W., 1993. Remobilisation of the continental lithosphere by a mantle plume: major-, trace-element, and Sr-, Nd-, and Pb-isotope evidence from picritic and tholeiitic lavas of the Noril'sk District, Siberian Trap, Russia. Contributions to Mineralogy and Petrology 114, 171–188.

McDonough, W.F., McCulloch, M.T., Sun, S.S., 1985. Isotopic and geochemical systematic in Tertiary–Recent basalts from southeastern Australia and implications for the evolution of the sub-continental lithosphere. Geochimica et Cosmochimica Acta 49, 2051–2067.

Mahoney, J., Coffin, M., 1997. Large igneous provinces: continental, oceanic, and planetary volcanism. Geophysics Monograph, vol. 100. American Geophysical Union, p. 438.

Pirajno, F., 2000. Ore deposits and mantle plumes. Kluwer Academic Publication, p. 556.

Pirajno, F., Mao, J., Zhang, Z., Zhang, Z., Chai, F., 2008. The association of mafic–ultramafic intrusions and A-type magmatism in the Tian Shan and Altay orogens, NW China: implications for geodynamic evolution and potential for the discovery of new ore deposits. Journal of Asian Earth Sciences 32, 165–183.

Pirajno, F., Ernst, R.E., Borisenko, A.S., Fedoseev, G., Naumov, E.A., 2009. Intraplate magmatism in Central Asia and China and associated metallogeny. Ore Geology Reviews 35, 114–136.

Pouchou, J.L., Pichoir, F., 1991. Quantitative analysis of homogeneous or stratified microvolumes applying the model PAP. In: Heinrich, K.F.J., Newbury, D.E. (Eds.), Electron probe quantitation. Plenum Press, New York, pp. 31–75.

Putirka, K.D., 2005. Mantle potential temperatures at Hawaii, Iceland, and the mid-ocean ridge system, as inferred from olivine phenocrysts: evidence for thermally driven mantle plume. Geochemistry, Geophysics, Geosystems 6, Q05L08. doi:10.1029/2005GC000915.

Qi, L., Hu, J., Gregoire, D.C., 2000. Determination of trace elements in granites by inductively coupled plasma–mass spectrometry. Talanta 51, 507–513.

Reichow, M.K., Pringle, M.S., Al'Mukhamedov, A.I., Allen, M.B., Andreichev, V.L., Buslov, M.M., Davies, C.E., Fedoseev, G.S., Fitton, J.G., Inger, S., Medvedev, A.Y., Mitchell, C., Puchkov, V.N., Safonova, I. Yu., Scott, R.A., Saunders, A.D., 2009. The timing and extent of the eruption of the Siberian Traps large igneous province: implications for the end-Permian environmental crisis. Earth and Planetary Science Letters 277, 9–20.

Roeder, P.L., Emslie, R.F., 1970. Olivine-liquid equilibrium. Contributions to Mineralogy and Petrology 29, 275–289.

Rollinson, H.R., 1993. Using Geochemical Data: Evaluation, Presentation, Interpretation. Longmans, Singapore, p. 352.

Rudnick, R.L., Gao, S., 2003. Composition of the continental crust. In: Rudnick, R.L., (eds), The crust. Vol. 3 of Holland, H. D., and Turekian, K. K. (eds), Treatise on geochemistry. Oxford, Elsevier-Pergamon, pp.1–64.

Shellnutt, J.G., Zhou, M.F., 2007. Permian peralkaline, peraluminous and metaluminous A-type granites in the Panxi district, SW China: their relationship to the Emeishan mantle plume. Chemical Geology 243, 286–316.

Shu, L.S., Chen, Y., Lu, H., Charvet, J., Laurent, S., Yin, D., 2000. Paleozoic accretionary terranes in northern Tianshan, NW China. Geochemical Journal 19, 193–202.

Staudigel, H., Zindler, A., Hart, S.R., Leslie, T., Chen, C.Y., Clague, D., 1984. The isotope systematic of a juvenile intraplate volcano: Pb, Nd and Sr isotope ratios of basalts from Loihi Seamount, Hawaii. Earth and Planetary Science Letters 69, 13–29.

Sun, S.S., McDonough, W.F., 1989. Chemical and isotopic systematics of oceanic basalts: implications for mantle composition and processes. In: Saunders, A.D., Norry, M.J. (Eds.), Magmatism in the Ocean Basin: Geological Society, London, Special Publications, vol. 42, pp. 313–345.

Thompson, R.N., Gibson, S.A., 2000. Transient high temperatures in mantle plume heads inferred from magnesian olivines in Phanerozoic picrites. Nature 407, 502–506.

Ulmer, P., 1989. The dependence of the Fe2+–Mg cation-partitioning between olivine and basaltic liquid on pressure, temperature and composition. Contributions to Mineralogy and Petrology 101, 261–273.

Wang, C.Y., Zhou, M.F., Qi, L., 2007. Permian flood basalts and mafic intrusions in the Jinping (SW China)–Song Da (northern Vietnam) district: Mantle sources, crustal contamination and sulfide segregation. Chemical Geology 243, 317–343.

Weaver, B.L., 1991. The origin of ocean island basalt end-member compositions: trace element and isotopic constraints. Earth and Planetary Science Letters 104, 381–397.

Weaver, J.S., Langmuir, C.H., 1990. Calculation of phase equilibrium in mineral melt systems. Computers & Geosciences 16, 1–19.

Wilson, M., 1989. Igneous Petrogenesis. InHarper Collins Academic, London, p. 466.

Winchester, J.A., Floyd, P.A., 1977. Geochemical discrimination of different magma series and their differentiation products using immobile elements. Chemical Geology 20, 325–343.

Xia, L.Q., Xu, X.Y., Xia, Z.C., 2003. Carboniferous post-collisional rift volcanic rocks in the Tianshan Mountains, northwestern China. Acta Geologica Sinica 77, 338–360.

Xiao, W.J., Windley, B.F., Chen, H.L., 2002. Carboniferous–Triassic subduction and accretion in the western Kunlun, China: implications for the collisional and accretionary tectonics of the northern Tibet plateau. Geology 30, 295–298.

Xiao, W.J., Windley, B.F., Liu, D.Y., 2005. Accretionary tectonics of the Western Kunlun Orogen, China: a Paleozoic–early Mesozoic, long-lived active continental margin with implications for the growth of southern Eurasia. Journal of Geology 113, 687–705.

Xinjiang Bureau of Geology and Mineral Resources (XJBGMR), 1993. Regional geology of the Xinjiang Uygur Autonomous Region. Geological Publishing House, Beijing. (in Chinese).

Xu, Y.G., Chung, S.L., Jahn, B.M., Wu, G.Y., 2001. Petrologic and geochemical constraints on the petrogenesis of Permian-Triassic Emeishan flood basalts in southwestern China. Lithos 58, 145–168.

Yang, S.F., Chen, H.L., Dong, C.W., Jia, C.Z., Wang, Z.G., 1996. The discovery of Permian syenite inside Tarim basin and its geodynamic significance. Geochemica 25, 121–128 (in Chinese with English abstract).

Yang, S.F., Chen, H.L., Ji, D.W., Li, Z.L., Dong, C.W., Jia, C.Z., Wei, G.Q., 2005. Geological process of early to middle Permian magmatism in Tarim basin and its geodynamic significance. Geological Journal of China Universities 11, 504–511 (in Chinese with English abstract).

Yang, S.F., Li, Z.L., Chen, H.L., Chen, W., Yu, X., 2006a. ^{40}Ar–^{39}Ar dating of basalts from Tarim Basin, NW China and its implication to a Permian thermal tectonic event. Journal of Zhejiang University-Science (Supp. II) 7, 170–174.

Yang, S.F., Li, Z.L., Chen, H.L., Xiao, W.J., YX., Lin, X.B., Shi, X.G., 2006b. Discovery of a Permian quartz syenitic porphyritic dyke from the Tarim Basin and its tectonic implications. Acta Petrologica Sinica 22, 1405–1412.

Yang, S.F., Li, Z., Chen, H., Santosh, M., Dong, C.W., Yu, X., 2007. Permian bimodal dyke of Tarim Basin, NW China: geochemical characteristics and tectonic implications. Gondwana Research 12, 113–120.

Yin, H., Huang, S., Zhang, K., Hansen, H.J., Yang, F., Ding, M., Bie, X., 1992. The effects of volcanism of the Permo-Triassic mass extinction in South China. In: Sweet, W.C., Yang, Z.Y., Dickins, J.M., Yin, H.F. (Eds.), Permo-Triassic Events in the Eastern Tethys: Stratigraphy, Classification, and Relations with the Western Tethys. World and Regional Geology, vol. 2. Cambridge University Press, Cambridge, pp. 146–157.

Zhang, S.B., 2003. A Guide to the Stratigraphic Investigation on the Periphery of the Tarim Basin. Petroleum Industry Press, p. 280 (In chinese).

Zhang, H.F., Sun, M., Lu, F.X., Zhou, X.H., Zhou, M.F., Liu, Y.S., Zhang, G.H., 2001. Moderately depleted lithospheric mantle underneath the Yangtze Block: evidence from a garnet lherzolite xenolith in the Dahongshan kimberlite. Geochemical Journal 35, 315–331.

Zhang, C.L., Li, X.H., Li, Z.X., Ye, H.M., Li, C.N., 2008. A Permian layered intrusive complex in the Western Tarim Block, Northwestern China: product of a Ca. 275-Ma mantle plume? Journal of Geology 116, 269–287.

Zhou, M.F., Malpas, J., Song, X., Kennedy, A.K., Robinson, P.T., Sun, M., Lesher, M., Keays, R.R., 2002. A temporal link between the Emeishan large igneous province (SW China) and the end-Guadalupian mass extinction. Earth and Planetary Science Letters 196, 113–122.

Zhou, M.F., Lesher, C.M., Yang, Z.X., Li, J.W., Sun, M., 2004. Geochemistry and petrogenesis of 270 Ma Ni–Cu-(PGE) sulfide-bearing mafic intrusions in the Huangshan district, eastern Xinjiang, northwest China: implications for the tectonic evolution of the Central Asian orogenic belt. Chemical Geology 209, 233–257.

Zhou, D.W., Liu, Y.Q., Xin, X.J., Hao, J.R., Dong, Y.P., Ouyang, Z.J., 2006. Formation of the Permian basalts and implications of geochemical tracing for paleo-tectonic setting and regional tectonic background in the Turpan-Hami and Santanghu basins, Xinjiang. Sciences in China (D) 49, 584–596.

Zhou, M.F., Arndt, N.T., Malpas, J., Wang, C.Y., Kennedy, A.K., 2008. Two magma series and associated ore deposit types in the Permian Emeishan Large Igneous Province, SW China. Lithos 103, 352–368.

Zindler, A., Hart, S., 1986. Chemical geodynamics. Annual Review of Earth and Planetary Sciences 14, 493–571.